

Transient-Safe and Attack-Resilient Secondary Control in AC Microgrids Under Polynomially Unbounded FDI Attacks

Mohamadamin Rajabinezhad, Nesa Shams, Yichao Wang, and Shan Zuo

Abstract—This letter proposes a novel, fully distributed, transient-safe resilient secondary control strategies for AC microgrids, addressing unbounded false data injection (FDI) attacks on control input channels. Unlike existing methods that focus primarily on steady-state convergence, our approach guarantees transient safety, ensuring that system states remain within predefined safety bounds even during attack initiation—a critical aspect overlooked in prior research. Given the reduction of network inertia by increasing the penetration of inverted-based renewables, large overshooting and intense fluctuations are more likely to occur during transients caused by disturbances and cyber attacks. To mitigate these risks, the proposed control method enhance defense capabilities against polynomially unbounded FDI attacks, maintaining safe system trajectories for both frequency and voltage throughout the transient response. Through rigorous Lyapunov-based stability analysis, we formally certify the strategies to achieve uniformly ultimately bounded (UUB) convergence in frequency and voltage regulation, and active power sharing across multi-inverter-based AC microgrids. Numerical simulation studies verify the effectiveness of the proposed control protocols, demonstrating improved system reliability, safety and resilience under adverse conditions.

I. INTRODUCTION

Microgrids play a vital role in integrating distributed energy resources (DERs) and managing the variability of renewables like wind and solar. They can operate independently or alongside the main grid, combining DERs, energy storage, and loads to enhance control, efficiency, and reliability [1], [2]. However, islanded microgrids face challenges due to the absence of traditional system inertia, making voltage and frequency stability more difficult to maintain. As microgrids evolve towards distributed operation, they depend on distributed control systems with local sensing and sparse communication networks [3]. While these systems improve efficiency and responsiveness, they also create vulnerabilities to cyberattacks, such as false data injection (FDI) attacks, which can bypass detection and have severe consequences [4]. Several approaches have been proposed for enhancing resilient control in AC microgrids. For instance, [4] introduces a secondary frequency control method that utilizes a resilience index to counteract state-dependent FDI cyber-attacks. Most studies consider disturbances, noise, faults, or attacks in AC

microgrids as bounded signals. However, recent works [5]–[8] show that attackers, leveraging quantum computing’s rapid capabilities, can launch unbounded false data injections. These attacks threaten the stability and integrity of cybersystems, highlighting the critical need for resilient defense strategies in AC microgrids. In [8], we proposed strategies to mitigate the effects of polynomially unbounded FDI attacks on control input channels and communication link faults.

However, as far as we know, the frequency and voltage regulation in Microgrids considering the two important performance metrics “resiliency” and “safety” simultaneously, remains largely unexplored. This is particularly crucial for inverter-based microgrids, where the low-inertia nature leads to significant frequency fluctuations, potentially breaching system protection thresholds. Therefore, in designing control policies for frequency and voltage regulation, it is essential to ensure that frequency and voltage remains within safe limits throughout operation, preventing excessive deviations from the desired value [9]–[11]. The classical method, model predictive control (MPC), handles dynamic constraints but is computationally demanding, often requiring reduced model orders in MG secondary control, compromising stability and safety. MPC also struggles with nonlinearities and communication issues [10]. Recently, control barrier functions (CBFs) have emerged as an effective tool for ensuring safety in systems like collision avoidance in automated vehicles, and robotics trajectory planning [12]. This inspires the development of a CBF-based safe controller for frequency and voltage regulation in microgrids [9], [10]. The letter’s contributions are outlined as follows:

- We propose a novel, fully distributed transient-safe and attack-resilient secondary control strategies for AC microgrids that are designed to ensure both safety and resilience against polynomially unbounded FDI attacks, even during transient response. These strategies incorporate a compensational signal with adaptively tuned parameters based on neighborhood relative information, effectively addressing both frequency and voltage regulation. Unlike previous methods which primarily focus on steady-state convergence and only could handle a limited range of unbounded attacks with bounded first-order time derivatives [5]–[7], our approach guarantees that system states remain within predefined safety bounds during transient responses even under wider range of unbounded FDI attacks signals by only requiring bounded higher-order time derivatives, which is less restrictive compared with the similar

Mohamadamin Rajabinezhad, Nesa Shams (Upcoming Student), Yichao Wang, and Shan Zuo are with the Department of Electrical and Computer Engineering, University of Connecticut, 371 Fairfield Way; U-4157 Storrs, Connecticut 06269-4157 U.S.A. (Emails: mohamadamin.rajabinezhad@uconn.edu; nashams71@gmail.com; yichao.wang@uconn.edu; shan.zuo@uconn.edu.)

requirement found in the existing literature. This is crucial for mitigating large overshooting and intense fluctuations due to reduced network inertia and cyber attacks.

- We conduct a rigorous Lyapunov-based stability analysis to prove that our strategies ensure uniformly ultimately bounded (UUB) convergence for frequency, voltage regulation, and power sharing. The analysis confirms that the strategies maintain transient safety even under polynomially unbounded FDI attacks, mitigate adverse effects, and manage fault impacts effectively. By adjusting adaptation gains, we can make the ultimate bounds for frequency and voltage arbitrarily small, enhancing safety and stability.

- The fully distributed defense strategies require no global information, ensuring scalability and easy integration. Their effectiveness in maintaining transient safety and stability is validated through simulations on a modified IEEE 34-bus test feeder system with inverter-based resources, demonstrating significant improvements in reliability and transient-safety under adverse conditions.

II. PRELIMINARIES ON GRAPH THEORY AND NOTATIONS

Consider a network with N inverters and one leader node, which operates autonomously due to the absence of incoming edges. Followers process information from adjacent agents. The network is represented by $\mathcal{G} = (\mathcal{V}, \mathcal{E}, \mathcal{A})$, where \mathcal{V} is the node set, $\mathcal{E} \subset \mathcal{V} \times \mathcal{V}$ is the edge set, and $\mathcal{A} = [a_{ij}] \in \mathbb{R}^{N \times N}$ is the adjacency matrix with a_{ij} as the edge weight: $a_{ij} \neq 0$ if $(v_j, v_i) \in \mathcal{E}$, otherwise $a_{ij} = 0$. There are no repeated edges or self-loops, so $a_{ii} = 0$. Define $\mathcal{D} = \text{diag}(d_i) \in \mathbb{R}^{N \times N}$ and $\mathcal{L} = \mathcal{D} - \mathcal{A}$ as the in-degree and Laplacian matrices, respectively, where $d_i = \sum_{j=1}^N a_{ij}$. Pinning gain g_i represents the influence of the leader on the i -th converter: $g_i > 0$ if there is a link, $g_i = 0$ otherwise. The matrix $\mathcal{G} = \text{diag}(g_i)$ represents the pinning gains. Denote $\mathcal{L} + \mathcal{G} = \mathcal{L}_{\mathcal{G}}$. \mathcal{F} and \mathcal{L} are the sets $\{1, 2, \dots, N\}$ and $\{N + 1, N + 2\}$. $\mathbf{1}_N$ is a column vector of ones. \otimes , $\text{diag}\{\cdot\}$, and $\|\cdot\|$ denote the Kronecker product, block diagonal matrix, and Euclidean norm, respectively.

A. Safety Preliminaries

In this section, we present the preliminaries of the CBF, a powerful tool for designing safe controllers. Consider the following affine nonlinear system:

$$\dot{x} = f(x) + g(x)u \quad (1)$$

where the functions f and g are locally Lipschitz continuous. Here, $x \in \mathbb{R}^n$ represents the state of the system, and $u \in \mathbb{R}^m$ is the control input.

Definition 1. [12]. A continuous function $\alpha : [-b, a) \rightarrow [-\infty, +\infty)$ is said to be an extended class K function for $a, b > 0$ if it is strictly increasing and $\alpha(0) = 0$.

Definition 2. [13]. A set Ω is forward invariant for system (1) if its solutions starting at all $x(t_0) \in \Omega$ satisfy $x(t) \in \Omega$ for $\forall t \geq t_0$.

Definition 3. [12]. Consider a set $\Omega = \{x \in \mathbb{R}^n \mid h(x) \geq 0\}$ for a continuously differentiable function $h : \mathbb{R}^n \rightarrow$

\mathbb{R} . The function h is termed a control barrier function if there exists an extended class K function α such that $\sup_{u \in \mathbb{R}^m} \{L_f h(x) + L_g h(x)u + \alpha(h(x))\} \geq 0$, where $L_f h(x) = \frac{\partial h}{\partial x} f(x)$, $L_g h(x) = \frac{\partial h}{\partial x} g(x)$ are the Lie derivatives, and $\alpha(\cdot)$ is an extended class K function.

Lemma 1. ([12]). For a CBF $h(x)$, define the set for $x \in \mathbb{R}^n$, $K_{cbf}(x) = \{u \in \mathbb{R}^m : L_f h(x) + L_g h(x)u + \alpha(h(x)) \geq 0\}$.

Then, any Lipschitz continuous controller $u \in K_{cbf}(x)$, will render the set $\Omega = \{x \in \mathbb{R}^n : h(x) \geq 0\}$ forward invariant for control system (1).

III. STANDARD CONSENSUS CONTROL IN ISOLATED AC MICROGRIDS

In islanded microgrids, feedback linearization decouples voltage and frequency dynamics. Secondary control [3] adjusts setpoints for decentralized primary control by providing frequency ω_{n_i} and voltage V_{n_i} setpoints through neighbor data exchange. Using droop control, the frequency and voltage are defined as $\omega_i = \omega_{n_i} - m_{P_i} P_i$, and $v_{odi} = V_{n_i} - n_{Q_i} Q_i$. The dynamics of this droop-based regulation in secondary control are modeled as in [3], [6].

$$\dot{\omega}_{n_i} = \dot{\omega}_i + m_{P_i} \dot{P}_i = u_{f_i}, \quad (2)$$

$$\dot{V}_{n_i} = \dot{v}_{odi} + n_{Q_i} \dot{Q}_i = u_{v_i}, \quad (3)$$

Here, P_i and Q_i represent the active and reactive powers, respectively, while ω_i is the operating angular frequency, and v_{odi} refers to the d -axis component of the inverter terminal voltage after the abc to $dq0$ transformation. The droop coefficients m_{P_i} and n_{Q_i} correspond to the $P - \omega$ and $Q - v$ relationships, determined based on the inverters' power ratings. The auxiliary control inputs u_{f_i} and u_{v_i} will be designed later. The setpoints ω_{n_i} and V_{n_i} are obtained by integrating u_{f_i} and u_{v_i} over time, which in turn regulates ω_i and v_{odi} through the droop control dynamics. The local cooperative frequency and voltage control protocols at each inverter will be designed based on the following relative information with respect to the neighboring inverters and the leaders

$$\xi_{f_i} \equiv c_f \left(\sum_{j \in \mathcal{F}} a_{ij} (\omega_j - \omega_i) + g_i (\omega_k - \omega_i) \right) \quad (4)$$

$$+ \sum_{j \in \mathcal{F}} a_{ij} (m_{P_j} P_j - m_{P_i} P_i),$$

$$\xi_{v_i} \equiv c_v \left(\sum_{j \in \mathcal{F}} a_{ij} (v_{odj} - v_{odi}) + g_i (v_k - v_{odi}) \right) \quad (5)$$

$$+ \sum_{j \in \mathcal{F}} a_{ij} (n_{Q_j} Q_j - n_{Q_i} Q_i),$$

where c_f and c_v are constant coupling gains. Since the inverters have identical parameters, the same coupling gains are used for the neighborhood relative information at each inverter. The variables ω_k and v_k represent the frequency reference and voltage reference values, respectively. Denote $\omega_{n_k} = \omega_k + m_{P_i} P_i$ and $V_{n_k} = v_k + n_{Q_i} Q_i$. Utilizing the neighborhood information from Eqs. (4) and (5) [3], the standard cooperative secondary control protocols for AC microgrids are expressed as $\dot{\omega}_{n_i} = u_{f_i}^c = \xi_{f_i}$ and $\dot{V}_{n_i} = u_{v_i}^c = \xi_{v_i}$.

The global vector forms of (4) and (5) are

$$\xi_f = -c_f \mathcal{L}_G (\omega_n - \mathbf{1}_N \otimes \omega_{n_k}), \quad (6)$$

$$\xi_v = -c_v \mathcal{L}_G (V_n - \mathbf{1}_N \otimes V_{n_k}), \quad (7)$$

where $\xi_f = [\xi_{f_1}^T, \dots, \xi_{f_N}^T]^T$, $\xi_v = [\xi_{v_1}^T, \dots, \xi_{v_N}^T]^T$, $\omega_n = [\omega_{n_1}^T, \dots, \omega_{n_N}^T]^T$ and $V_n = [V_{n_1}^T, \dots, V_{n_N}^T]^T$. Define the global frequency and voltage containment error vectors as

$$e_f = \omega_n - (\mathcal{L}_G^{-1}) \mathcal{L}_G (\mathbf{1}_N \otimes \omega_{n_k}), \quad (8)$$

$$e_v = V_n - (\mathcal{L}_G^{-1}) \mathcal{L}_G (\mathbf{1}_N \otimes V_{n_k}). \quad (9)$$

A. Modeling of Unbounded Attacks

In this part, we introduce the unbounded FDI attacks on the local control inputs of the frequency and voltage control loops, then auxiliary control input signal in (2) and (3) becomes to:

$$\bar{u}_{f_i} = u_{f_i} + \Delta_{f_i}, \quad (10)$$

$$\bar{u}_{v_i} = u_{v_i} + \Delta_{v_i}, \quad (11)$$

where \bar{u}_{f_i} and \bar{u}_{v_i} are corrupted inputs, Δ_{f_i} and Δ_{v_i} denote the polynomially unbounded attack signals injected to the control inputs of frequency and voltage control loops at the i^{th} inverter, respectively.

Assumption 1. *The attack signals $\Delta_{f_i} \in C^\gamma$ and $\Delta_{v_i} \in C^\gamma$ are polynomially unbounded with the finite polynomial order of γ . That is, $|\Delta_{f_i}^{(\gamma)}| \leq \kappa_{f_i}$ and $|\Delta_{v_i}^{(\gamma)}| \leq \kappa_{v_i}$, where $\gamma > 0$ is a scalar, and κ_{f_i} and κ_{v_i} are positive constants.*

Remark 1. *Assumption 1 considers a broader range of unbounded FDI attacks, potentially exploiting quantum computational advantages. Unlike [5]–[7], it relaxes the bounded first-order derivative requirement to a bounded higher-order derivative. The proposed controller handles both time-varying and constant signals if $|\Delta_{f_i}^{(\gamma)}| \leq \kappa_{f_i}$ and $|\Delta_{v_i}^{(\gamma)}| \leq \kappa_{v_i}$, with γ being adjustable depending on the defender's computational power. Polynomially unbounded attacks may cause rapid changes, potentially leading to system instability before saturation limits are reached.*

Definition 4 ([6]). *Signal $x(t) \in \mathbb{R}^n$ is UUB with an ultimate bound b , if there exist positive constants b and c , independent of $t_0 \geq 0$, and for every $a \in (0, c)$, there exists $t_1 = t_1(a, b) \geq 0$, independent of t_0 , such that $\|x(t_0)\| \leq a \Rightarrow \|x(t)\| \leq b, \forall t \geq t_0 + t_1$.*

The following assumptions are needed for the communication graph topology to guarantee cooperative consensus.

Assumption 2. *There exists a directed path from the leader to each inverter.*

IV. PROBLEM FORMULATION

Even though the primary controller is designed to stabilize the microgrid, introducing a secondary controller can affect the system's dynamic behavior and stability. Hence, it is essential to ensure that the transient stability of the closed-loop microgrid system is maintained when the secondary controller is implemented. In this work, we are to design a control approach for frequency and voltage regulations in microgrid while considering resilient distributed control and

safety even during the unbounded FDI attacks. Meanwhile, a designated safe region can be established around the desired operating point, and we intend to ensure that the frequency and voltage of all inverters remain within this region at all times during operation to satisfy the goal of safety. The transient safety bound is primarily influenced by safety considerations and the physical limitations of the hardware, and is generally larger than the steady-state bound. However, to the authors' best knowledge, there still lacks a commonly accepted standard suggesting the magnitude of transient safety bound for microgrids. Consequently, we adopt the steady-state bound as the transient bound for DER output voltages and frequency as $[0.9, 1.1] p.u.$ and $60 \pm 2 Hz$ respectively [10]. Specifically, the safety constraints for frequency and voltage are given by

$$-\omega_l \leq \hat{\omega}_i \leq \omega_h, \quad -v_l \leq \hat{v}_i \leq v_h \quad (12)$$

where $\hat{\omega}_i = \omega_i - \omega_{ref}$ and $\hat{v}_i = v_i - v_{ref}$. Also, $\omega_l > 0$, $\omega_h > 0$, $v_l > 0$, and $v_h > 0$ which define the safety regions for frequency and voltage.

A. Safety Guarantees With Control Barrier Functions

Throughout the operation, the frequency of each inverter must stay within the defined safety limits, which are governed by the constraints in (12). Subsequently, we introduce two functions h_{f_i} and h_{v_i} as follows:

$$h_{f_{1,i}} = \hat{\omega}_i + \omega_l \quad h_{f_{2,i}} = \omega_h - \hat{\omega}_i \quad (13)$$

$$h_{v_{1,i}} = \hat{v}_i + v_l \quad h_{v_{2,i}} = v_h - \hat{v}_i \quad (14)$$

Hence, to guarantee the safety of frequency is equivalent to ensuring that the following inequalities hold:

$$h_{f_{1,i}} > 0, \quad h_{f_{2,i}} > 0, \quad h_{v_{1,i}} > 0, \quad h_{v_{2,i}} > 0,$$

which result in a safety set:

$$\Omega_{f_i} = \{\hat{\omega} \mid h_{f_{1,i}} \geq 0, h_{f_{2,i}} \geq 0\}$$

$$\Omega_{v_i} = \{\hat{v} \mid h_{v_{1,i}} \geq 0, h_{v_{2,i}} \geq 0\}$$

As a result, when Ω_{f_i} and Ω_{v_i} are forward invariant, the frequency and voltage safety constraints are satisfied. Now, consider the control barrier functions $h_{f_{1,i}}$ and $h_{f_{2,i}}$, with their derivatives given by $\dot{h}_{f_{1,i}} = \dot{\omega}_i$ and $\dot{h}_{f_{2,i}} = -\dot{\omega}_i$. To guarantee the forward invariance of the set Ω_{f_i} , the extended class \mathcal{K} functions α_1 and α_2 are chosen as linear functions, specifically:

$$\alpha_1 : h_{f_{1,i}} \rightarrow \eta_1 h_{f_{1,i}}, \quad \alpha_2 : h_{f_{2,i}} \rightarrow \eta_2 h_{f_{2,i}} \quad (15)$$

where $\eta_1 > 0$ and $\eta_2 > 0$. For the Ω_{v_i} the procedure is the same. Following Lemma 1, the conditions resulting from CBFs for safe control are given by:

$$\dot{h}_{f_{1,i}} + \eta_1 h_{f_{1,i}} \geq 0, \quad \dot{h}_{f_{2,i}} + \eta_1 h_{f_{2,i}} \geq 0 \quad (16)$$

Substituting $h_{f_{1,i}} = \hat{\omega}_i$ and $h_{f_{2,i}} = -\hat{\omega}_i$ into (16), and using (2), we see the condition (16) actually contains the term $m_{pi} \dot{P}_i$, which is unknown for us. Therefore, this condition cannot be used to search for the safe control directly. Further, we note that the load fluctuation in the real world is not unlimited. Thus, it is reasonable to assume that the disturbance is bounded by a positive constant d_s [9]. Then the conditions for safe control resulting from robust control barrier functions are given by

$$u_{f_i} - m_{pi} d_s + \eta_1 (\omega_i + \omega_l - \omega_{ref}) \geq 0, \quad (17)$$

$$-u_{f_i} + m_{pi}d_s + \eta_2(\omega_h - \omega_i + \omega_{ref}) \geq 0, \quad (18)$$

That is, if the control $u_{f_i}^{safe}$ is designed to satisfy conditions (16), the safety can be guaranteed. The control input u_{f_i} is computed by solving the following optimization problem:

$$\begin{aligned} \min_{u_{f_i}^{safe} \in \mathbb{R}} J(u(t)) &= \int_{t_0}^{t_f} \left(\frac{1}{2} (u_{f_i}^{safe}(t) - u_{f_i}^c(t))^2 \right) dt \\ \text{s.t.} & \quad (17) \text{ and } (18) \end{aligned} \quad (19)$$

Note that the variable in the optimization problem (19) is $u_{f_i}^{safe}$, and (17) and (18) are actually linear constraints. Thus the optimization (19) is a quadratic programming (QP) problem and can be further rewritten as

$$\arg \min_{u_{f_i}^{safe}} \|u_{f_i}^{safe} - u_{f_i}^c\|_2 \quad (20)$$

$$\text{s.t. } A_{cbf} u_{f_i}^{safe}(t) \leq b_{cbf}$$

where $A_{cbf} = [-1; 1]$ and $b_{cbf} = [\eta_1(\omega_i + \omega_l - \omega_{ref}) - m_{pi}d_s; m_{pi}d_s + \eta_2(\omega_h - \omega_i + \omega_{ref})]$. The optimization problem designed ensures that the control input adheres to safety constraints while minimizing deviations from the reference control input. Denote $\Delta u_{f_i} \equiv u_{f_i}^{safe} - u_{f_i}^c$. This approach enables efficient computation of the control input, upholding both system safety and resilience. The QP problem can be solved rapidly, allowing real-time control to be achieved [9]. Due to space constraints, the voltage problem formulation is omitted, but it follows the same structure as the frequency formulation.

Remark 2. In the QP problem, the objective function $\|u_{f_i} - u_{f_i}^c\|$ is a measure of how close u_{f_i} is to $u_{f_i}^c$. The boundedness of $\|u_{f_i} - u_{f_i}^c\|$ is guaranteed because the QP problem is solved over a feasible set defined by the constraints $A_{cbf} u_{f_i}(t) \leq b_{cbf}$. These constraints ensure that the feasible region for u_{f_i} is bounded. As a result, the minimum value of $\|u_{f_i} - u_{f_i}^c\|$ is finite, making Δu_{f_i} bounded due to the constrained, bounded nature of the optimization problem.

B. Resilient control Problem Formulation

In the face of polynomially unbounded FDI attacks, the objective of resilient frequency and voltage control is to design the control inputs u_{f_i} and u_{v_i} such that the local frequency ω_i and voltage v_{odi} of each inverter converge to a small vicinity around the reference values set by the the leader.

Lemma 2 ([3], [6]). *Given Assumptions 2, the resilient frequency and voltage consensus control objectives are achieved if $e_f(t)$ and $e_v(t)$ are UUB, respectively.*

We now present the resilient defense problems for the secondary control loops governing frequency and voltage.

Definition 5. *The Resilient Frequency and Voltage Defense Problem involves designing resilient control inputs, u_{f_i} and u_{v_i} , as specified in Eqs. (2) and (3), respectively, to ensure the resilient frequency and voltage control objectives are met. Specifically, both the global frequency containment error e_f , defined in Eq. (8), and the global voltage containment error e_v , defined in Eq. (9), should remain UUB despite unbounded*

attacks on the local frequency and voltage control input channels.

V. FULLY DISTRIBUTED RESILIENT DEFENSE STRATEGIES DESIGN

We propose the following fully distributed resilient defense strategies to solve the resilient frequency and voltage defense problems. we have $u_{f_i} = u_{f_i}^{safe} + \Gamma_{f_i}$. Given $u_{f_i}^c = \xi_{f_i}$ and $\Delta u_{f_i} \equiv u_{f_i}^{safe} - u_{f_i}^c$, this can be expressed as follows:

$$\begin{cases} u_{f_i} = \xi_{f_i} + \Delta u_{f_i} + \Gamma_{f_i}, \\ \Gamma_{f_i} = \frac{\xi_{f_i} \Upsilon_{f_i}}{|\xi_{f_i}| + \eta_{f_i}}, \\ \Upsilon_{f_i}^{(\gamma)} = \nu_{f_i} |\xi_{f_i}| \end{cases} \quad \begin{cases} u_{v_i} = \xi_{v_i} + \Delta u_{v_i} + \Gamma_{v_i}, \\ \Gamma_{v_i} = \frac{\xi_{v_i} \Upsilon_{v_i}}{|\xi_{v_i}| + \eta_{v_i}}, \\ \Upsilon_{v_i}^{(\gamma)} = \nu_{v_i} |\xi_{v_i}| \end{cases} \quad (21)$$

where, η_{f_i} and η_{v_i} are positive, exponentially decaying functions that facilitate a smooth control strategy for practical implementation. Γ_{f_i} and Γ_{v_i} represent compensatory signals, while Υ_{f_i} and Υ_{v_i} are adaptively tuned parameters. The adaptation gains ν_{f_i} and ν_{v_i} are fixed positive constants, and the initial values of both Υ_{f_i} and Υ_{v_i} are also positive.

Theorem 1. *Based on Assumptions 2 and 1, and applying the cooperative resilient frequency defense strategies outlined in Eq. (4) and Eq. (21), the global frequency containment error e_f , as defined in Eq. (8), remains UUB, thus solving the resilient frequency defense problem. Moreover, by appropriately increasing the adaptation gain ν_{f_i} , as indicated in Eq. (21), the ultimate bound of e_f can be reduced to an arbitrarily small value.*

Proof: Combining (6), (10), (4) and (21) yields the vector form:

$$\dot{\xi}_f = -c_f \mathcal{L}_G \dot{\omega}_n = -c_f \mathcal{L}_G \times (\xi_f + \Delta_f + \Delta u_f + \Gamma_f), \quad (22)$$

where $\xi_f = [\xi_{f_1}^T, \dots, \xi_{f_N}^T]^T$, $\Delta_f = [\Delta_{f_1}^T, \dots, \Delta_{f_N}^T]^T$, $\Delta u_f = [\Delta u_{f_1}^T, \dots, \Delta u_{f_N}^T]^T$ and $\Gamma_f = [\Gamma_{f_1}^T, \dots, \Gamma_{f_N}^T]^T$. Consider the following Lyapunov function

$$E = \xi_f^T \mathcal{L}_G^{-1} \xi_f. \quad (23)$$

The time derivative of (23) is

$$\begin{aligned} \dot{E} &= 2\xi_f^T \mathcal{L}_G^{-1} \dot{\xi}_f \\ &= \xi_f^T \times 2\mathcal{L}_G^{-1} \left(-c_f \mathcal{L}_G (\xi_f + \Delta_f + \Delta u_f + \Gamma_f) \right) \\ &= -2c_f \xi_f^T \xi_f - 2c_f \xi_f^T \Delta_f - 2c_f \xi_f^T \Delta u_f - 2c_f \xi_f^T \Gamma_f \\ &\leq -2c_f \sum_{i \in \mathcal{F}} \xi_{f_i}^2 + 2c_f \sum_{i \in \mathcal{F}} |\xi_{f_i}| (|\Delta_{f_i}| + |\Delta u_{f_i}|) \\ &\quad - 2c_f \sum_{i \in \mathcal{F}} (\xi_{f_i} \Gamma_{f_i}). \end{aligned} \quad (24)$$

After substituting Γ_{f_i} as defined in (21), Eq. (24) becomes

$$\begin{aligned} \dot{E} &\leq -2c_f \sum_{i \in \mathcal{F}} \xi_{f_i}^2 + 2c_f \sum_{i \in \mathcal{F}} \left(|\xi_{f_i}| (|\Delta_{f_i}| + |\Delta u_{f_i}|) \right. \\ &\quad \left. - (|\xi_{f_i}|^2 \times \Upsilon_{f_i}) / (|\xi_{f_i}| + \eta_{f_i}) \right) \\ &= -2c_f \sum_{i \in \mathcal{F}} \xi_{f_i}^2 + 2c_f \sum_{i \in \mathcal{F}} \left(|\xi_{f_i}|^2 (|\Delta_{f_i}| + |\Delta u_{f_i}|) - |\xi_{f_i}|^2 \right. \\ &\quad \left. \times \Upsilon_{f_i} + |\xi_{f_i}| |\Delta_{f_i}| \eta_{f_i} + |\xi_{f_i}| |\Delta u_{f_i}| \eta_{f_i} \right) / (|\xi_{f_i}| + \eta_{f_i}). \end{aligned} \quad (25)$$

Per Assumption 1 and note that η_{f_i} is a exponentially decaying function and the decay rate of η_{f_i} exceeds the growth rate of polynomially unbounded signals, we have $\lim_{t \rightarrow \infty} (|\xi_{f_i}| |\Delta_{f_i}| \eta_{f_i}) = \lim_{t \rightarrow \infty} (|\xi_{f_i}| |\Delta u_{f_i}| \eta_{f_i}) = 0$. Furthermore, noting that $(-2c_f \sum_{i \in \mathcal{F}} \xi_{f_i}^2)$ is negative, and Δu_{f_i} is bounded and can be disregarded compared to Δ_{f_i} , which is polynomially unbounded signal, design Υ_{f_i} as in (21), then when $|\xi_{f_i}| > \kappa_{f_i} / \nu_{f_i}$, $\exists t_1$, such that

$$\begin{aligned} 2c_f \sum_{i \in \mathcal{F}} \left(|\xi_{f_i}|^2 (|\Delta_{f_i}| + |\Delta u_{f_i}|) - |\xi_{f_i}|^2 \times \Upsilon_{f_i} \right) \\ / (|\xi_{f_i}| + \eta_{f_i}) \leq 0, \forall t \geq t_1. \end{aligned} \quad (26)$$

Define the compact set $\Psi_i \equiv \{|\xi_{f_i}| \leq \kappa_{f_i} / \nu_{f_i}\}$. Considering (25) and (26), we obtain that outside the compact set Ψ_i , $\dot{E} \leq 0$, $\forall t \geq t_1$. By LaSalle's invariance principle [14], we obtain that ξ_f is UUB. From Theorem 4.18 of [15], the upper bound is a class \mathcal{K} function of κ_{f_i} / ν_{f_i} . Therefore, the larger the value of the adaptation gain ν_{f_i} , the smaller the ultimate bound. Note that $\xi_f = -c_f \mathcal{L}_G e_f$. Hence e_f is also UUB. This completes the proof.

Remark 3. Although, the larger the values of ν_{f_i} , the smaller the ultimate bound, excessively high gains ν_{f_i} lead to overshoot, instability, control accuracy reduction, etc. Moderate gains balance responsiveness and stability, ensuring effective control.

Theorem 2. Given Assumptions 2 to 1, and using the cooperative resilient voltage defense strategies delineated by Eq. (5) and Eq. (21), the global voltage containment error e_v defined in Eq. (9), is UUB, i.e., the resilient voltage defense problem is solved. Furthermore, by properly incrementing the adaptation gain ν_{v_i} in (21), the ultimate bound of e_v can be rendered arbitrarily small.

Proof: Note that $\xi_v = -c_v \mathcal{L}_G e_v$. The approach used to prove Theorem 2 mirrors the one of Theorem 1.

VI. VALIDATION AND RESULTS

A 50-Hz islanded, three-phase inverter-based AC microgrid is utilized to assess the proposed fully distributed, transient-safe resilient secondary defense strategies. Fig. 1 shows the microgrid setup, which consists of four inverter-based distributed generators (DGs) and two loads. The detailed dynamics of each inverter, described in [3] and [16]. The parameters for a microgrid test system are as follows: m_P

and n_Q are 9.4×10^{-5} and 1.3×10^{-3} for DGs 1 and 2, and 18.8×10^{-5} and 2.6×10^{-3} for DGs 3 and 4. Transmission line parameters are: resistances $R_{12} = 0.23 \Omega$, $R_{23} = 0.35 \Omega$, $R_{34} = 0.23 \Omega$, and inductances $L_{12} = 318 \mu H$, $L_{23} = 847 \mu H$, $L_{34} = 318 \mu H$. Loads have resistances of 3Ω and inductances of $6.4 mH$ for Load 1 and $12.8 mH$ for Load 2. The proposed control defense strategy is demonstrated in Matlab Simulink through two case studies. The inverters communicate on a bidirectional communication network with the adjacency matrix of $\mathcal{A} = [0 \ 1 \ 0 \ 1; 1 \ 0 \ 1 \ 0; 0 \ 1 \ 0 \ 1; 1 \ 0 \ 1 \ 0]$. The pinning gains are $g_{15} = 1$. The frequency and voltage reference, are 60 Hz, and 340 V, respectively.

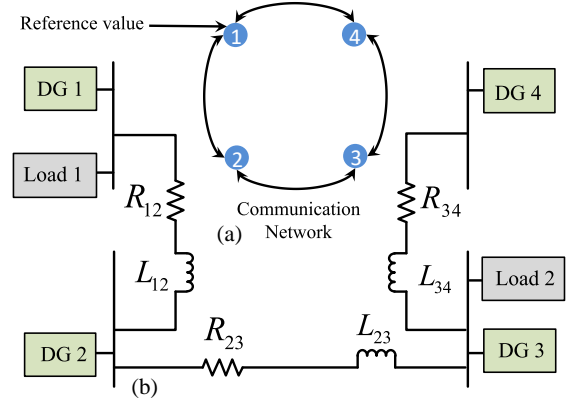


Fig. 1. Cyber-physical microgrid system: (a) Communication graph topology among four inverters and two leaders (references), (b) Microgrid test setup.

A. Case Study I: Resilience Against the Unbounded Attacks without safety constraints

In this case study, the unbounded attack injections to the frequency and voltage control loops are $\Delta_{f_1} = 2t^2 + 10$, $\Delta_{f_2} = 2.5t^2 + 12$, $\Delta_{f_3} = -1.5t^2 + 6$, $\Delta_{f_4} = -3t^2 - 12$ and $\Delta_{v_1} = 1.5t^2 + 50$, $\Delta_{v_2} = 3t^2 + 15$, $\Delta_{v_3} = -2t^2 + 30$, $\Delta_{v_4} = 2t^2 + 50$, respectively. The performance of the resilient defense strategies, as defined in (21), is evaluated in the condition with out considering the transient-safety constraints. The constant gains $c_f = 20$, $c_v = 10$, and the adaptation gains for the resilient defense strategies are set at $\nu_{v_i} = 20$, $\nu_{f_i} = 350$, $i = 1, 2, 3, 4$. η_{v_i} and η_{f_i} are determined as $e^{-\alpha_{v_i}}$ and $e^{-\alpha_{f_i}}$, respectively, where $\alpha_{v_i} = \alpha_{f_i} = 0.01$, $i = 1, 2, 3, 4$. Figure 2 contrast the voltage and frequency of each DGs responses to the unbounded attacks using resilient defense strategies without considering the safety constraints. Also Figure 3 indicate the phase plot of the trajectory of voltage and frequency during the simulation time span. The results indicate that while the resilient secondary defense strategies yield favorable outcomes—such as inverter voltages stabilizing near 340 V and frequency aligning with the 60 Hz reference—the transient response of both voltage and frequency violates the safety limits after unbounded FDI attacks are initiated at $t = 5$ s, due to the absence of safety constraints.

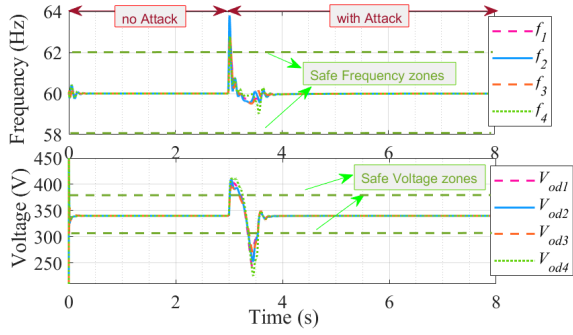


Fig. 2. Performance of the resilient fully distributed resilient secondary defense strategies in Case I: frequency and voltage performance.

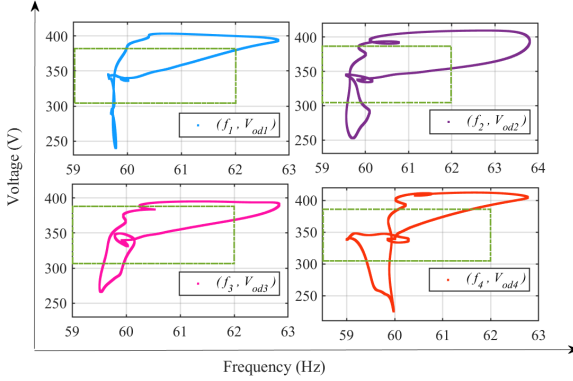


Fig. 3. Trajectory of DG's output voltages and frequency using the resilient control strategy without transient-safety.

B. Case Study II: Transient-Safe and Resilience Against the Unbounded Attacks

In the second case study the safety constraints also being considered. The proposed transient-safety resilient secondary defense strategies lead to favorable results: inverter voltages stabilize within small neighbour of 340 V and frequency aligns with the 60 Hz reference. Besides, the frequency and voltage at all buses always keep in the safe regions during the whole process including the initiation of unbounded FDI attacks on control input. These outcomes validate the proposed resilient and safe control approach's ability to ensure UUB convergence in frequency and voltage regulation in multi-inverter-based AC microgrids under polynomially unbounded attacks and keep the voltage and frequency in a predefined safe region all during the process operation.

VII. CONCLUSION

This letter presents novel, fully distributed, transient-safe and attack-resilient secondary control strategies for AC microgrids that address polynomially unbounded FDI attacks on control input channels. Unlike existing methods that only guarantee steady-state resilience for limited range of unbounded attacks, our approach ensures transient safety by keeping system states within predefined bounds during wider range of unbounded attacks and disturbances. It enhances defense against risks associated with reduced network inertia

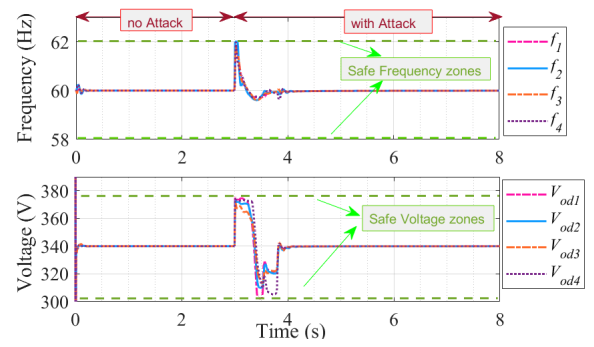


Fig. 4. Performance of the proposed fully distributed transient-safety resilient secondary defense strategy in Case II: frequency and voltage performance.

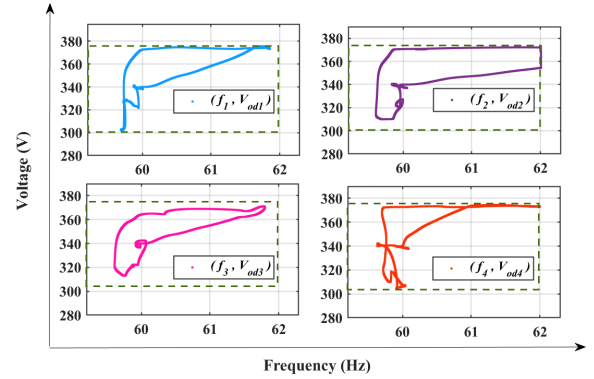


Fig. 5. Trajectory of DG's output voltages and frequency using the proposed transient-safe and resilient control strategy

caused by increasing penetration of inverted-based renewables, such as overshooting and fluctuations. The strategies ensure UUB convergence for frequency and voltage regulation, and active power sharing, with stability proven through Lyapunov analysis. Adaptation gains, ν_{f_i} and ν_{V_i} , can be tuned to refine UUB stability. Simulations on a modified IEEE 34-bus system demonstrate improved reliability, safety, and resilience under adverse conditions.

REFERENCES

- [1] J. M. Guerrero, J. C. Vasquez, J. Matas, L. G. De Vicuña, and M. Castilla, "Hierarchical control of droop-controlled ac and dc microgrids—a general approach toward standardization," *IEEE Transactions on industrial electronics*, vol. 58, no. 1, pp. 158–172, 2010.
- [2] M. Rajabinezhad, H. Firoozi, H. Khajeh, and H. Laaksonen, "Chapter 3—electrical energy storage devices for active buildings," *Active Building Energy Systems*; Springer: Cham, Switzerland, 2021.
- [3] A. Bidram, A. Davoudi, F. L. Lewis, and Z. Qu, "Secondary control of microgrids based on distributed cooperative control of multi-agent systems," *IET Generation, Transmission & Distribution*, vol. 7, no. 8, pp. 822–831, 2013.
- [4] M. Jamali, M. S. Sadabadi, M. Davari, S. Sahoo, and F. Blaabjerg, "Resilient cooperative secondary control of islanded ac microgrids utilizing inverter-based resources against state-dependent false data injection attacks," *IEEE Transactions on Industrial Electronics*, vol. 71, no. 5, pp. 4719–4730, 2023.
- [5] X.-K. Liu, S.-Q. Wang, M. Chi, Z.-W. Liu, and Y.-W. Wang, "Resilient secondary control and stability analysis for DC microgrids under mixed cyber attacks," *IEEE Transactions on Industrial Electronics*, 2023.

- [6] S. Zuo, O. A. Beg, F. L. Lewis, and A. Davoudi, "Resilient networked AC microgrids under unbounded cyber attacks," *IEEE Trans. Smart Grid*, vol. 11, no. 5, pp. 3785–3794, 2020.
- [7] D. Zhou, Q. Zhang, F. Guo, Z. Lian, J. Qi, and W. Zhou, "Distributed resilient secondary control for islanded DC microgrids considering unbounded FDI attacks," *IEEE Trans Smart Grid*, 2023.
- [8] Y. Wang, M. Rajabinezhad, and S. Zuo, "Secondary defense strategies of ac microgrids under polynomially unbounded fdi attacks and communication link faults," *IEEE Control Systems Letters*, 2024.
- [9] J. Zhang, L. Ding, X. Lu, and W. Tang, "A novel real-time control approach for sparse and safe frequency regulation in inverter intensive microgrids," *IEEE Transactions on Industry Applications*, 2023.
- [10] Z. Ma, Q. Zhang, and Z. Wang, "Safe and stable secondary voltage control of microgrids based on explicit neural networks," *IEEE Transactions on Smart Grid*, vol. 14, no. 5, pp. 3375–3387, 2023.
- [11] T. Zhao, J. Wang, and M. Yue, "A barrier-certificated reinforcement learning approach for enhancing power system transient stability," *IEEE Transactions on Power Systems*, vol. 38, no. 6, pp. 5356–5366, 2023.
- [12] A. D. Ames, X. Xu, J. W. Grizzle, and P. Tabuada, "Control barrier function based quadratic programs for safety critical systems," *IEEE Transactions on Automatic Control*, vol. 62, no. 8, pp. 3861–3876, 2016.
- [13] W. Xiao, C. Belta, and C. G. Cassandras, "Decentralized merging control in traffic networks: A control barrier function approach," in *Proceedings of the 10th ACM/IEEE International Conference on Cyber-Physical Systems*, 2019, pp. 270–279.
- [14] M. Krstic, P. V. Kokotovic, and I. Kanellakopoulos, *Nonlinear and adaptive control design*. John Wiley & Sons, Inc., 1995.
- [15] H. K. Khalil, *Nonlinear Systems, Third Edition*. Upper Saddle River, NJ: Prentice Hall, 2002.
- [16] S. Zuo, A. Davoudi, Y. Song, and F. L. Lewis, "Distributed finite-time voltage and frequency restoration in islanded AC microgrids," *IEEE Transactions on Industrial Electronics*, vol. 63, no. 10, pp. 5988–5997, 2016.